A Weak Form Implementation of Nonlinear Axisymmetric Shell Equations With Examples

Matteo Pezzulla

Flexible Structures Laboratory,
Department of Mechanical Engineering,
Institute of Mechanical Engineering,
École Polytechnique Fédérale de Lausanne,
Lausanne 1015, Switzerland
e-mail: matteo.pezzulla@epfl.ch

Pedro M. Reis[1]

Flexible Structures Laboratory,
Department of Mechanical Engineering,
Institute of Mechanical Engineering,
École Polytechnique Fédérale de Lausanne,
Lausanne 1015, Switzerland
e-mail: pedro.reis@epfl.ch

We present a weak form implementation of the nonlinear axisymmetric shell equations. This implementation is suitable to study the nonlinear deformations of axisymmetric shells, with the capability of considering a general mid-surface shape, non-homogeneous (axisymmetric) mechanical properties and thickness variations. Moreover, given that the weak balance equations are arrived to naturally, any external load that can be expressed in terms of an energy potential can, therefore, be easily included and modeled. We validate our approach with existing results from the literature, in a variety of settings, including buckling of imperfect spherical shells, indentation of spherical and ellipsoidal shells, and geometry-induced rigidity (GIR) of pressurized ellipsoidal shells. Whereas the fundamental basis of our approach is classic and well established, from a methodological view point, we hope that this brief note will be of both technical and pedagogical value to the growing and dynamic community that is revisiting these canonical but still challenging class of problems in shell mechanics.
[DOI: 10.1115/1.4044816]

1 Introduction

Shells are among the most iconic slender structures, as they can exhibit highly nonlinear mechanical responses and undergo a variety of instabilities [1]. One of the canonical shell problems is the buckling of a pressurized spherical shell, where the structure collapses catastrophically as soon as the pressure reaches a critical value. An analytical prediction for the critical buckling pressure for a perfect spherical shell was first computed in 1915 by Zoelly [2], following a linear stability analysis, and later verified with more refined theories [1,3]. Focusing our attention on linearly elastic materials, a variety of shell theories have been derived stemming from different kinematic assumptions; for example, the Donnell–Mushtari–Vlasov (DMV) [4] and Budiansky-Sanders (or moderate-rotation) [5] theories. Even though this plethora of shell theories has led to the understanding of many engineering-relevant phenomena, such as the determination of the critical buckling

pressure of spherical shells, there is only a limited number of problems where one can make progress through purely analytical methods [6,7], especially for shells with a generalized shape or non-homogeneous properties. As such, the need for numerical implementations of the shell equations has been made clear long ago, and several computational approaches have been proposed and have became well established. These numerical strategies include the weak form implementation of 2D nonlinear shell equations (e.g., as provided by commercial packages such as ABAQUS) or systems of ODEs in the case of axisymmetric shells when using the infinitesimal stain and moderate rotation constructions [8,9].

Even though shell theories and well-defined engineering problems that said theories target to solve have been around for over a century, during the past few years, there has been a revived interest in this class of problems, including the development of novel fabrication techniques [10] that have enabled more controlled experiments [11,12]. In particular, these experiments have further clarified and enabled a precise and systematic quantification of the effect of defects on dictating the strength of spherical shells. Consequently, there has been a revival of numerical methods that can efficiently solve the nonlinear shell equations, with a particular emphasis on the buckling and indentation of spherical shells containing engineered small defects [8,11]. The method developed in Ref. [13] is based on the Budiansky–Sanders theory and is tailored for (axisymmetric) spherical shells with small defects. This method involves solving a system of six ODEs in a highly efficient manner, but the Young's modulus and the thickness profiles were limited to be homogeneous even though the model could have been readily adapted to treat analytic (axisymmetric) non-homogeneous profiles.

Here, we propose an alternative to the different methods already present in the literature, comprising a weak form implementation of the nonlinear axisymmetric linearly elastic shell equations, valid for small strains and presenting no restrictions on the magnitude of the displacements and rotations as developed in Ref. [7]. The underlying equations that we tackle are standard and well established but the way we frame them enables for an efficient and easy treatment of axisymmetric shells of arbitrary shape, non-homogeneous elastic properties and thickness profile. In addition, any load, either mechanical or otherwise, can be readily considered, as long as it can be represented by a reduced energy functional. From a practical sense, this framework is also enticing because it can be readily implemented in commercial multiphysics simulation software, such as COMSOL, for numerical analysis. We validate this model with existing experimental and numerical results from the literature on the buckling and indentation of spherical shells [11,12], as well as on the geometry-induced rigidity of both spherical and ellipsoidal shells that are pressurized [14,15].

2 Nonlinear Axisymmetric Shell Equations Revisited

For the sake of convenience and completeness, even if classic and well established, we start by reviewing the nonlinear model for axisymmetric linearly elastic shells with no restriction on the magnitude of displacements and rotations [7]. Let $\mathcal{S} = \mathbf{r}(\eta^1, \eta^2)$ be a 2D surface embedded in $\mathbb{R}^3$ and parameterized by $y = (\eta^1, \eta^2)$. We adopt the standard notation that Greek indices α, β, ... take values in $\{1, 2\}$, whereas Latin indices i, j, ... run from 1 to 3. The parametrization of $\mathcal{S}$ enables us to define (covariant) tangent vectors as

$$\mathbf{a}_\alpha = \mathbf{r}_{,\alpha} \equiv \frac{\partial \mathbf{r}}{\partial \eta^\alpha} \tag{1}$$

as well as the induced surface metric $a_{\alpha\beta}$ (first fundamental form)

$$a_{\alpha\beta} = \mathbf{a}_\alpha \cdot \mathbf{a}_\beta = a_{\beta\alpha} \tag{2}$$

where "·" denotes the Euclidean inner product on $\mathbb{R}^3$. The inverse metric is defined via $a^{\alpha\gamma} a_{\gamma\beta} = \delta^\alpha_\beta$, where summation is implied over repeated indices and δ^α_β denotes the Kronecker delta. The metric and its inverse map between co- and contravariant quantities, e.g., the contravariant form of $\mathbf{a}_1$ is $\mathbf{a}^1 = a^{1\alpha} \mathbf{a}_\alpha$. The unit-length normal vector $\mathbf{a}_3$, which can be identified with the unit outward normal $\mathbf{n}$,

is defined by $\mathbf{a}_3 \equiv \mathbf{a}^3 = (\mathbf{a}_1 \times \mathbf{a}_2)/|\mathbf{a}_1 \times \mathbf{a}_2|$. The second fundamental form $b_{\alpha\beta}$ is given by

$$b_{\alpha\beta} = \mathbf{n} \cdot \mathbf{a}_{\alpha,\beta} \qquad (3)$$

We denote the middle surface of the shell in its undeformed configuration as $\overset{\circ}{\mathcal{S}} = \overset{\circ}{\mathbf{r}}(s, \phi)$, where $s \in [0, s_{\max}]$ and $\phi \in [0, 2\pi)$. By using Eqs. (2) and (3), we compute the first and second fundamental forms of the undeformed middle surface $\overset{\circ}{\mathbf{a}}$ and $\overset{\circ}{\mathbf{b}}$. Similarly, quantities without the accent will refer to the deformed middle surface of the shell $\mathcal{S} = \mathbf{r}(s, \phi)$. Consequently, the strain and bending tensors can be defined as

$$E_{\alpha\beta} = \frac{1}{2}(a_{\alpha\beta} - \overset{\circ}{a}_{\alpha\beta}), \qquad K_{\alpha\beta} = b_{\alpha\beta} - \overset{\circ}{b}_{\alpha\beta} \qquad (4)$$

Denoting the thickness of the shell by h, the elastic energy of a linearly elastic shell can then be expressed as [7]

$$\mathcal{U} = \int \frac{Eh}{2(1-\nu^2)}[(1-\nu)E_\alpha^\beta E_\beta^\alpha + \nu E_\alpha^\alpha E_\beta^\beta]\,\mathrm{d}\overset{\circ}{\omega}$$
$$+ \int \frac{Eh^3}{24(1-\nu^2)}[(1-\nu)K_\alpha^\beta K_\beta^\alpha + \nu K_\alpha^\alpha K_\beta^\beta]\,\mathrm{d}\overset{\circ}{\omega} \qquad (5)$$

where $\mathrm{d}\overset{\circ}{\omega} = \sqrt{|\det(\overset{\circ}{a}_{\alpha\beta})|}\,\mathrm{d}y = \overset{\circ}{a}\,\mathrm{d}y$.

In the specific examples that we will focus on in Sec. 4, the Young's modulus and the thickness will be assumed to be homogeneous and $s_{\max} = \pi/2$. Therefore, we normalize the energy in Eq. (5) by $E/(16\pi(1-\nu^2))$ and introduce the trace operator in the undeformed metric "tr", to rewrite the energy as

$$\overline{\mathcal{U}} = h\int_0^{\pi/2}[(1-\nu)\mathrm{tr}(\mathbf{a} - \overset{\circ}{\mathbf{a}})^2 + \nu\mathrm{tr}^2(\mathbf{a} - \overset{\circ}{\mathbf{a}})]\overset{\circ}{a}\,\mathrm{d}s$$
$$+ \frac{h^3}{3}\int_0^{\pi/2}[(1-\nu)\mathrm{tr}(\mathbf{b} - \overset{\circ}{\mathbf{b}})^2 + \nu\mathrm{tr}^2(\mathbf{b} - \overset{\circ}{\mathbf{b}})]\overset{\circ}{a}\,\mathrm{d}s \qquad (6)$$

where $\eta^1 = s$ is the coordinate going along the profile curve from the north pole. The undeformed middle surface is represented by a profile curve given by $\overset{\circ}{\mathbf{r}}(s, \phi) = \overset{\circ}{\mathbf{r}}(s) = (\overset{\circ}{\phi}(s), \overset{\circ}{\psi}(s))$, whereas the parametrization of the deformed profile curve can be written as $\mathbf{r}(s) = (\phi(s), \psi(s))$. We then derive the first and second fundamental forms for the deformed surface as

$$\mathbf{a} = \begin{pmatrix} \phi_s^2 + \psi_s^2 & 0 \\ 0 & \phi^2 \end{pmatrix}$$
$$\mathbf{b} = \frac{1}{\sqrt{\phi_s^2 + \psi_s^2}}\begin{pmatrix} \psi_{ss}\phi_s - \phi_{ss}\psi_s & 0 \\ 0 & \phi\psi_s \end{pmatrix} \qquad (7)$$

and the same expressions with the accent hold for the undeformed surface. The energy in Eq. (6) is a second-order functional of the two functions, $\phi(s)$ and $\psi(s)$, defined on the real segment $[0, \pi/2]$. For symmetry, we require that $\phi(0) = \psi_s(0) = 0$, whereas the clamp at the equator considered in our examples imposes $\phi(\pi/2) = R$ and $\phi_s(\pi/2) = 0$.

2.1 Specification of the Loads. In what follows, we will focus on two types of loads: (i) live pressure and (ii) point indentation at the north pole of the shell. The potential associated with the (live) pressure can be written as $\mathcal{P} = p\Delta V$, where a positive pressure causes a negative variation in volume (compression) of the shell. Neglecting the term proportional to the initial volume (since it does not enter the balance equations), the potential can be recast via the divergence theorem as

$$\mathcal{P}_\mathrm{p} = p\frac{1}{3}\int \mathbf{r} \cdot \mathbf{n}\,\mathrm{d}\omega = \frac{p}{3}\int_0^{\pi/2}\phi(\psi\phi_s - \psi_s\phi)\,\mathrm{d}s \qquad (8)$$

With regard to the point force indentation f at the north pole, the potential can be written as

$$\mathcal{P}_\mathrm{f} = \int_0^{\pi/2} f\,\delta(s)w\,\mathrm{d}s \qquad (9)$$

where $\delta(s)$ is the Dirac delta function and $w = (\mathbf{r} - \overset{\circ}{\mathbf{r}}) \cdot \mathbf{n}$ represents the normal displacement. Appropriately normalizing the load potentials by $E/(16\pi(1-\nu^2))$, the total energy becomes $\overline{\mathcal{U}}_\mathrm{tot} = \overline{\mathcal{U}} + \overline{\mathcal{P}}_\mathrm{p} + \overline{\mathcal{P}}_\mathrm{f}$.

3 Numerical Method

Equilibrium equations are generated by imposing $\delta\overline{\mathcal{U}}_\mathrm{tot} = 0$, for all possible variations $\delta\phi$ and $\delta\psi$. We numerically minimize the functional by discretizing the domain in 100 intervals, using Hermite cubic shape functions for the unknown fields $\tilde{\phi} = \phi - \overset{\circ}{\phi}$ and $\tilde{\psi} = \psi - \overset{\circ}{\psi}$, via the Newton–Raphson method. In the specific illustrative problems considered in Sec. 4, the deflection at the pole increases monotonically, while the pressure or the force can be non-monotonic. For this reason, and similarly to what was also done previously in Ref. [8], we treat p and f as unknowns and the displacement at the pole as the loading parameter.

We use the commercial package COMSOL MULTIPHYSICS (v. 5.2, COMSOL Inc.) to automatically generate the balance equations and solve them via the Newton–Raphson method. However, we note that the procedure presented could also be implemented in custom-made codes, given that the balance equations in weak form could be obtained by hand, albeit resulting in cumbersome expressions, or via a symbolic mathematical software such as MATHEMATICA or MAPLE.

In COMSOL, within the environment "weak form PDE," the weak form is discretized using Hermite cubic shape functions, ensuring the continuity of second derivatives that appear in curvatures. This discretization yields a nonlinear algebraic system in the nodal values of $\tilde{\phi}$ and $\tilde{\psi}$, which is then solved via a standard Newton–Raphson solver. When the problem involves two sequential loading stages, e.g., first depressurizing the shell and then indenting it at the north pole, the weak form is solved in two sequential steps, where the initial conditions of the second step coincide with the solution of the first step. Hereon, we will refer to solutions of this model as the *1D model*.

4 Results

Having introduced our framework and the numerical method, we now apply it to several specific problems that illustrate the practical and technical value of our approach. We shall focus exclusively on spherical and ellipsoidal shells, for which $\overset{\circ}{\phi}(s) = a\sin(s)$ and $\overset{\circ}{\psi}(s) = b\cos(s)$.

We start by validating the model by comparing the results for two cases: (a) the buckling of imperfect spherical shells discussed in Refs. [11,16] and (b) the indentation of depressurized spherical shells presented in Ref. [12] that were numerically solved in Ref. [8]. We point the reader to the Refs. [8,11,12,16] for a more detailed account and a contextualization of these problems. In both cases (a) and (b), we have that $a = b = R$. In case (a), we consider defects at the north pole having the shape of Gaussian dimple, introduced as a normal displacement of the middle surface by $w_\mathrm{I} = -\delta e^{-(s/\beta_0)^2}$, where δ is the radial amplitude of the defect and β is the angular width of the defect [8,11]. To compare our results obtained through COMSOL with those in Ref. [11], we also use the dimensionless parameter that characterizes the imperfect shell
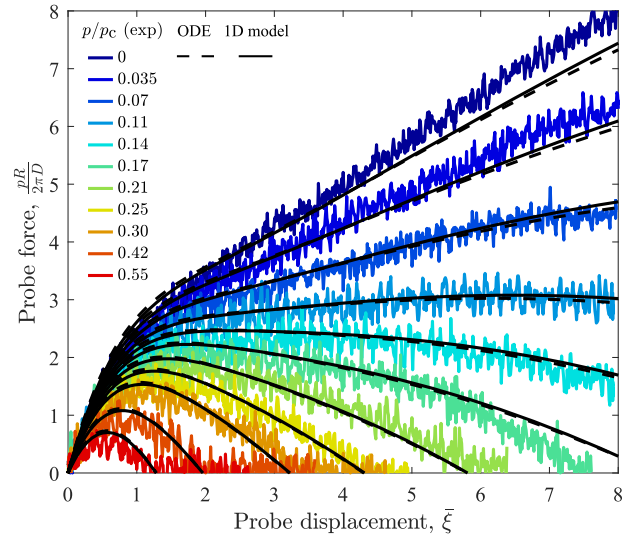
$$\lambda = 12(1-\nu^2)^{1/4}(R/h)^{1/2}\beta_0$$

In Fig. 1(a), we present the normalized pressure p/p_c, where $p_c = 2E/\sqrt{3(1-\nu^2)}$ is the buckling pressure obtained by Zoelly [2], as a function of the displacement of the north pole, normalized by
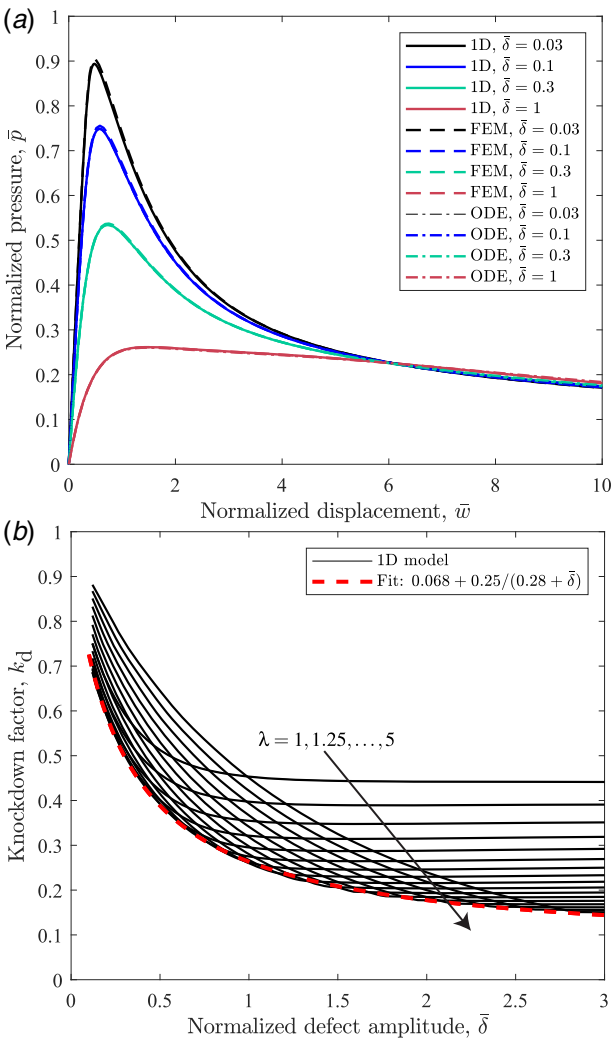
Fig. 1 Buckling of imperfect spherical shells: (a) normalized pressure versus normalized displacement for different normalized defect amplitudes δ̄ via FEM (dashed lines) [11], ODEs obtained by Hutchinson (dashed dotted lines) [11] and the present 1D model (solid lines) and (b) knockdown factor versus δ̄ for different values of λ via the 1D model (solid black lines), the fitted envelope determined in Ref. [11] is plotted as the dashed line

Fig. 2 Indentation of a pressurized shell. The indentation force f, normalized by $2\pi D/R$, is plotted versus the normalized additional displacement at the north pole $\bar{\xi} = \sqrt{1-\nu^2}\,\Delta w_{\text{pole}}/h$ for different values of the internal pressure. The experimental data were extracted from Ref. [12] and were presented as the colored solid lines; the data from the ODE model were obtained by Hutchinson and Thompson [8] and is shown as the dashed lines; and the data from our 1D model were shown as the solid black lines.

the thickness of the shell. The results from our 1D model are reported in colored solid lines, whereas the results from FEM and ODE model by Hutchinson based on the Budiansky–Sanders theory are reported in dashed and dash-dotted lines, respectively. For each model, four different values of the defect amplitude were computed, namely $\bar{\delta} = \delta/h = (0.03, 0.1, 0.3, 1)$, and excellent agreement is observed among the three methods, thereby indicating the validity of our approach. We now investigate wider ranges of the normalized defect amplitude ($0 \le \bar{\delta} \le 3$) and λ (in steps of $\Delta\lambda = 0.25$). In Fig. 1(b), we plot the associated knockdown factors (defined as the ratio between the buckling pressure of an imperfect shell to the buckling pressure of the equivalent perfect shell) as a function of $\bar{\delta}$. The solid black lines are the results from the presented 1D model for $\lambda \in [1, 5]$, and they show the emergence of a plateau for the knockdown factor that, above a critical defect amplitude depending on λ, becomes insensitive to the defect. This plot was already shown in Refs. [11,16] where a fitted envelope was proposed (red dashed curve). Again, the agreement among the data is excellent, as the set of curves from our 1D model all lies above in a way that is consistent with the previously computed envelope.

In Fig. 2, we present the results on the indentation at the north pole of a depressurized spherical shell, superposed on top of the experimental data that was reported in Ref. [12]. The plot shows the indentation force f, normalized by $2\pi D/R$ where $D = Eh^3/(12(1-\nu^2))$ is the bending stiffness, as a function of the normalized additional displacement at the north pole $\bar{\xi} = \sqrt{1-\nu^2}\,\Delta w_{\text{pole}}/h$ for different values of the internal pressure. The experimental data from Ref. [12] are reported in solid colored lines and the ODE results from Ref. [8] are depicted in dashed black lines, whereas the results from the 1D model are in solid black lines. As the pressure inside the shell is decreased, the structure is energetically closer to buckling and this translates into a smaller rigidity (the initial linear slope) and a lower peak of the indenting force. Note that the behavior is subcritical, meaning that the shell would buckle when the force reaches its maximum if the indenter was not glued to the shell. In the limit of $p/p_c \to 1$, an infinitesimal force would cause the shell to buckle (zero initial slope).

As a third and final illustrative example of our approach, we use the 1D model to study the geometry-induced (GIR) rigidity K of pressurized spherical and ellipsoidal shells. Restraining ourselves to axisymmetric deformations, this rigidity is defined and measured by indenting the shell at the north pole and measuring the slope of the force-displacement curve for different values of the internal pressure. Using our 1D model, we reproduced the results presented in Refs. [14,15], and we compare them with the theoretical prediction for the GIR derived in Ref. [14] via the DMV theory for spherical shells, which was then modified and proposed for ellipsoidal shells in Ref. [15]:

$$K = \frac{8D}{l_b^2}\frac{\pi(\tau^2-1)^{1/2}}{2\,\mathrm{arctanh}(1-\tau^{-2})^{1/2}} \qquad (10)$$

where $\tau = p/(4k_M^2\sqrt{EhD})$ is the dimensionless applied pressure, $l_b = (D/Ehk_M^2)$ is the local bending scale at the pole, and κ_M is the mean curvature of the shell at the pole. Figure 3 shows the dimensionless rigidity $K/\sqrt{k_M^2 EhD}$ versus the dimensionless pressure τ for ellipsoidal and spherical perfect shells, as predicted by Eq. (10) (solid black line) and by the 1D model (colored dashed lines), which we use to explore two ellipsoidal shells and one
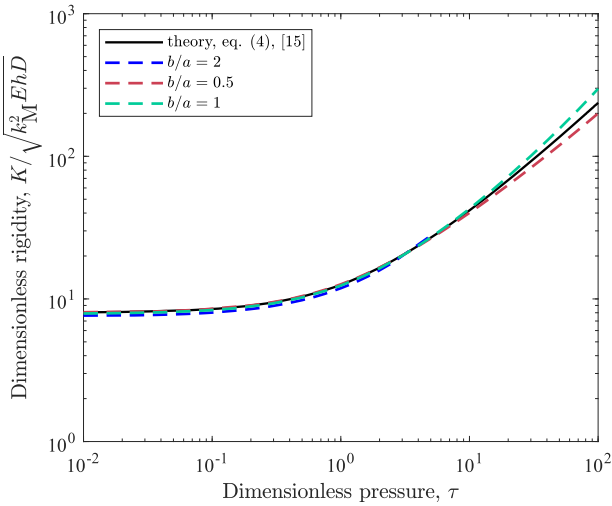
Fig. 3 Geometry-induced rigidity. Dimensionless rigidity $K/\sqrt{k_M^2 EhD}$ versus the dimensionless pressure τ for ellipsoidal and spherical perfect shells, as obtained via the 1D model (dashed colored lines) and the theoretical prediction from [15] (black line).

spherical shells, i.e., $a/b = 0.5, 1, 2$. The plot shows good agreement between the 1D model and the theory. Note that the numerical curves start to slightly deviate from theory for larger pressures. This mismatch is due to the eventual large stretching strains that the shell experiences for large pressures (beyond $\approx 5\%$). In particular, higher strains are attained for shells with higher values of the aspect ratio b/a. For example, the curve for $b/a = 2$ ends before $\tau = 10$ since the strains are too large (5–6%) for a linearly elastic shell model to be applicable.

To provide the reader with an idea about the computation time and convey the efficiency of our numerical implementation, a full pressure buckling simulation, with the normalized displacement at the north pole increasing from 0 to 10, takes approximately 3 s on a laptop with a 2.80 GHz quad-core processor and 16 GB of RAM. It is also important to notice that the weak form implementation enables the treatment of the three examples presented here by only changing the parameters defining the initial shape and activating/deactivating the different loads. As such, the examples explored above demonstrate the efficiency and versatility of our tool to address axisymmetric shell problems.

5 Concluding Remarks

We have presented a method to solve the nonlinear axisymmetric shell equations, in the case of linearly elastic materials, with no assumptions on the magnitude of the displacement and rotations.

The method is fast and efficient in handling an arbitrary axisymmetric shape, as well as any axisymmetric nonhomogeneity in the thickness and/or material properties. In this technical brief, we validated our approach with specific results for the buckling and indentation of spherical shells, and the GIR of ellipsoidal shells. Due to its formulation, the model can handle any mechanical and nonmechanical load, as long as it can be represented via an energy functional as in the case of natural curvature [17] or magnetic fields. The code can be made available upon request.

Acknowledgment

References

[1] Koiter, W. T., 1969, "The Nonlinear Buckling Behavior of a Complete Spherical Shell Under Uniform External Pressure, Parts I, II, III & IV," Proc. Kon. Ned. Ak. Wet., **B72**, pp. 40–123.
[2] Zoelly, R., 1915, "Ueber ein knickungsproblem an der kugelschale," Ph.D. thesis, ETH Zürich, Zürich, Switzerland.
[3] Hutchinson, J. W., 1967, "Imperfection Sensitivity of Externally Pressurized Spherical Shells," J. Appl. Mech., **34**(1), pp. 49–55.
[4] Donnell, L., 1977, *Beams, Plates and Shells*, McGraw Hill, New York.
[5] Sanders, J. L., 1963, "Nonlinear Theories for Thin Shells," Q. Appl. Math., **21**(1), pp. 21–36.
[6] Budiansky, B., 1968, "Notes on Nonlinear Shell Theory," J. Appl. Mech., **41**(35), pp. 393–401.
[7] Niordson, F., 1985, *Shell Theory*, Elsevier Science, Amsterdam.
[8] Hutchinson, J. W., and Thompson, J. M. T., 2017, "Nonlinear Buckling Interaction for Spherical Shells Subject to Pressure and Probing Forces," J. Appl. Mech., **84**(6), p. 061001.
[9] Hutchinson, J. W., and Thompson, J. M. T., 2018, "Imperfections and Energy Barriers in Shell Buckling," Int. J. Solids Struct., **148–149**, pp. 157–168.
[10] Lee, A., Brun, P.-T., Marthelot, J., Balestra, G., Gallaire, F., and Reis, P. M., 2016, "Fabrication of Slender Elastic Shells by the Coating of Curved Surfaces," Nat. Commun., **7**, p. 11155.
[11] Lee, A., López Jiménez, F., Marthelot, J., Hutchinson, J. W., and Reis, P. M., 2016, "The Geometric Role of Precisely Engineered Imperfections on the Critical Buckling Load of Spherical Elastic Shells," J. Appl. Mech., **83**(11), p. 111005.
[12] Marthelot, J., López Jiménez, F., Lee, A., Hutchinson, J. W., and Reis, P. M., 2017, "Buckling of a Pressurized Hemispherical Shell Subjected to a Probing Force," J. Appl. Mech., **84**(12), p. 121005.
[13] Hutchinson, J. W., 2016, "Buckling of Spherical Shells Revisited," P. Roy. Soc. A-Math. Phy., **472**(2195), p. 20160577.
[14] Vella, D., Ajdari, A., Vaziri, A., and Boudaoud, A., 2012, "Indentation of Ellipsoidal and Cylindrical Elastic Shells," Phys. Rev. Lett., **109**(14), p. 144302.
[15] Lazarus, A., Florijn, H. C. B., and Reis, P. M., 2012, "Geometry-Induced Rigidity in Nonspherical Pressurized Elastic Shells," Phys. Rev. Lett., **109**(14), p. 144301.
[16] López Jiménez, F., Marthelot, J., Lee, A., Hutchinson, J. W., and Reis, P. M., 2017, "Technical Brief: Knockdown Factor for the Buckling of Spherical Shells Containing Large-Amplitude Geometric Defects," J. Appl. Mech., **84**(3), p. 034501.
[17] Pezzulla, M., Stoop, N., Steranka, M. P., Bade, A. J., and Holmes, D. P., 2018, "Curvature-Induced Instabilities of Shells," Phys. Rev. Lett., **120**(4), p. 048002.